

Research Paper

Photoacoustic Imaging as an Early Biomarker of Radio Therapeutic Efficacy in Head and Neck Cancer

Laurie. J. Rich^{1,2}, Austin Miller³, Anurag K. Singh⁴, Mukund Seshadri^{1,2,5}✉

1. Laboratory for Translational Imaging, Department of Molecular and Cellular Biophysics and Biochemistry, Roswell Park Cancer Institute, Buffalo, New York 14263
2. Department of Pharmacology and Therapeutics, Roswell Park Cancer Institute, Buffalo, New York 14263
3. Department of Biostatistics and Bioinformatics, Roswell Park Cancer Institute, Buffalo, New York 14263
4. Department of Radiation Medicine, Roswell Park Cancer Institute, Buffalo, New York 14263
5. Department of Dentistry and Maxillofacial Prosthetics, Roswell Park Cancer Institute, Buffalo, New York 14263

✉ Corresponding author: Dr. Mukund Seshadri, Roswell Park Cancer Institute, Elm and Carlton streets, Buffalo, New York 14263. Ph: 716-845-1552; Email: Mukund.Seshadri@roswellpark.org.

© Ivyspring International Publisher. This is an open access article distributed under the terms of the Creative Commons Attribution (CC BY-NC) license (<https://creativecommons.org/licenses/by-nc/4.0/>). See <http://ivyspring.com/terms> for full terms and conditions.

Received: 2017.06.30; Accepted: 2018.01.19; Published: 2018.03.06

Abstract

The negative impact of tumor hypoxia on radiotherapeutic efficacy is well recognized. However, an easy to use, reliable imaging method for assessment of tumor oxygenation in routine clinical practice remains elusive. Photoacoustic imaging (PAI) is a relatively new imaging technique that utilizes a combination of light and ultrasound (US) to enable functional imaging of tumor hemodynamic characteristics *in vivo*. Several clinical trials are currently evaluating the utility of PAI in cancer detection for breast, thyroid, and prostate cancer. Here, we evaluated the potential of PAI for rapid, label-free, non-invasive quantification of tumor oxygenation as a biomarker of radiation response in head and neck cancer.

Methods: Studies were performed human papilloma virus- positive (HPV+) and -negative (HPV-) patient-derived xenograft (PDX) models of head and neck squamous cell carcinoma (HNSCC). PAI was utilized for longitudinal assessment of tumor hemodynamics (oxygenation saturation and hemoglobin concentration) before, during and after fractionated radiation therapy (fRT). Imaging datasets were correlated with histologic measures of vascularity (CD31), DNA damage (phosphorylated γ H2AX) and statistical modeling of tumor growth.

Results: A differential response to fRT was observed between HPV+ and HPV- xenografts. Temporal changes in tumor hemodynamics (oxygen saturation and hemoglobin concentration) measured by PAI showed significant association with treatment outcomes. PAI-based changes in oxygen saturation were detected within days after initiation of fRT prior to detectable change in tumor volume, highlighting the potential of PAI to serve as an early biomarker of therapeutic efficacy. Consistent with PAI results, immunohistochemical staining of vascularity (CD31) and DNA damage (phosphorylated γ H2AX) revealed distinct patterns of response in HPV+ and HPV- xenografts.

Conclusion: Collectively, our observations demonstrate the utility of PAI for temporal mapping of tumor hemodynamics and the value of PAI read-outs as surrogate measures of radiation response in HNSCC.

Key words: photoacoustic imaging, head and neck cancer, radiation, hypoxia, PDX

Introduction

Head and neck cancers represent a diverse group of malignancies that arise in multiple sites within this region [1]. A majority (~85%) of these cancers develop in the squamous lining of the mucosal surfaces in the aero-digestive tract, and are therefore histologically

referred to as squamous cell carcinoma (SCC) [2, 3]. Radiation therapy (RT), in combination with surgery and/or chemotherapy is often used in the management of head and neck SCC (HNSCC) patients [4, 5]. The lethal effects of RT are mediated through the

interaction of ionizing radiation with DNA, resulting in DNA damage that is chemically “fixed” in the presence of oxygen [6]. Under hypoxic conditions, this chemical fixation does not occur, reducing RT efficacy. It has been shown that the radiation dose necessary to achieve sufficient cell kill under hypoxic conditions is ~3 times higher than the dose required under oxygenated conditions [7]. This presents a significant hurdle to RT efficacy, as studies in pre-clinical rodent tumor models have shown the average fraction of cells growing under hypoxic conditions can be as high as 50% [8]. Consequently, both acute and chronic forms of hypoxia can limit the response of HNSCC to RT [9].

An extensive body of literature exists on the clinical value of measuring tumor oxygenation to prognosticate radiotherapeutic efficacy [10-12]. These studies have typically utilized immunostaining of tumor sections for hypoxia markers (e.g., CAIX, pimonidazole) [10], gene expression profiling of hypoxia-associated genes [11] and detection of DNA breaks to measure the hypoxic fraction of tumors [12]. Unfortunately, the invasive nature of these methods limits their ability to reliably monitor the temporal fluctuations in tumor oxygenation. Non-invasive imaging methods can overcome these limitations and allow for real-time imaging of dynamic changes in tumor oxygenation throughout the tumor. However, an easy to use, reliable imaging method for measuring tumor oxygenation in routine clinical practice remains elusive.

Photoacoustic imaging (PAI) is a hybrid imaging modality in which optical excitation (in the NIR region) locally heats the tissue, resulting in elastic expansion and generation of an acoustic signal [13, 14]. PAI exploits the optical absorption characteristics of hemoglobin (Hb) to provide quantitative estimates of both total Hb concentration (HbT) and oxygen saturation (sO₂), the amount of oxygen being carried by Hb [14]. The ability of PAI to non-invasively map and quantify tumor HbT and sO₂ levels without the need for exogenous contrast agents is an important benefit when compared to traditional radiologic methods such as MRI, PET or CT that rely on externally administered tracers. Given the ease of use, lack of ionizing radiation and relatively low cost of PAI, we hypothesized that PAI can be effectively utilized for frequent and repeated assessment of oxygenation in HNSCC before, during and after fractionated RT (fRT). In addition to traditional risk factors such as smoking and alcohol use, human papilloma virus (HPV) infection has also been implicated in the pathogenesis of oropharyngeal SCC [15]. It is now well recognized that patients with HPV-positive (HPV+) HNSCC are more responsive to

chemotherapy and RT than their HPV-negative (HPV-) counterparts [16, 17]. We therefore conducted experimental studies in both HPV+ and HPV- PDX models of HNSCC to assess the ability of PAI to monitor temporal changes in tumor oxygenation before the start of therapy, on-treatment and following RT. Our results demonstrate the utility of PAI for temporal mapping of tumor hemodynamics and highlight the potential of PAI-based estimates of oxygen saturation to serve as a biomarker of radiation response in HNSCC.

Materials and Methods

Animals

Experimental studies were carried out using eight to twelve-week-old female CB.17 (C.B-Igh-1^b/IcrTac-Prkdc^{scid}) severe combined immunodeficient (SCID) mice (Laboratory Animal Resource, RPCI) with an average body weight of ~20 g. Mice were kept in sterile micro isolator cages (4-5 mice per cage) in a pathogen-free environment and provided with standard chow/water and maintained on 12 h light/dark cycles in a HEPA-filtered environment. All experimental procedures were performed under aseptic conditions and in accordance with protocols approved by the Institutional Animal Care and Use Committee at Roswell Park Cancer Institute (RPCI).

Patient-derived xenograft models of HNSCC

De-identified tumor specimens were obtained under an approved Non-Human Subjects Research protocol at RPCI. Procured tumor tissue was transferred to the laboratory in RPMI media for transplantation into SCID mice. The HPV status of the donor tumor and the corresponding xenografts were confirmed by PCR and p16 immunohistochemistry.

Tumors were implanted subcutaneously in the leg for experimental studies using aseptic techniques as described previously [18].

Radiation treatment

Anesthetized mice were irradiated using the Philips RT 250 Orthovoltage X-ray unit (Philips Medical Systems, Andover, MA) equipped with an aluminum filter and operating at 75 kV/ 17.7 mA. The dose rate at this setting was ~0.68 Gy/min. Fractionated irradiation consisted of 3 Gy fractions delivered daily for five days for a total dose of 15 Gy. During irradiation, a ‘protective lead shield’ with an opening for the tumor was positioned over the animal to protect normal mouse tissue from exposure to radiation. Animals were monitored with a closed-circuit TV during irradiation and observed after completion of treatment to ensure full recovery.

Response assessment

Tumor volume was calculated using three-dimensional B-mode ultrasound (US) images as described below. Tumor volumes were acquired before, during and following treatment as an indicator of treatment response. During this time, animals were monitored for changes in body weight below 20% of pretreatment estimates, signs of morbidity, and euthanized as per institutionally approved protocols.

PAI with co-registered US of mice

Experimental PAI with co-registered US was performed using a commercially available laser integrated high-frequency ultrasound system (Vevo® LAZR, FujiFilm VisualSonics Inc., Toronto, Canada). The system consists of a tunable NIR Nd:YAG laser connected to a 256 element fiber-optic linear array hybrid US transducer, synchronized micro-ultrasound system and a work station to process and reconstruct the US/PA images. Mice were anesthetized using 2.5% Isoflurane (Philips Medical Systems, Andover, MA) and secured onto a heated imaging platform underneath the PAI transducer. Hair on the skin surface was removed and gel applied on top of the tumor to facilitate US transmission. PAI was performed using the following parameters: transducer, LZ-250; frequency, 21 MHz; depth, 20.00 mm; width, 23.04 mm; wavelength, 750/850 nm; gain, 18 dB for US and 43 dB for PAI; no persistence; PA focal depth, 10 mm; acquisition mode, sO₂/Hbt. Time gain compensation was applied to account for PA signal loss with increased depth and was kept constant for all imaging sessions. Acquisition parameters were kept constant for all imaging sessions throughout the study. Three-dimensional PA images were acquired for the whole tumor to obtain whole tumor estimates of tumor oxygen saturation (%sO₂) and hemoglobin concentration (HbT). Following imaging, animals were removed and monitored to ensure full recovery. Post-processing of all imaging data was performed using the Visualsonics® workstation suite (VevoLab, ver 1.7.2). Analysis was performed by tracing a region of interest (ROI) for the entire 3D region (>20 slices). B-mode US datasets were used to calculate tumor volume. PA-based estimates of %sO₂ and HbT were calculated using the two-wavelength approach as previously reported [19]. Color maps representing %sO₂ were displayed using a color look-up table superimposed on spatially co-registered B-mode US images.

Immunohistochemical staining of tumor sections

Tumor tissues were excised and placed in zinc fixative (BD Biosciences, San Diego, CA) for 24 h prior

to being embedded in paraffin. Tissues were sectioned at a thickness of 4 μm, mounted on positively charged slides, and stained for CD31/alpha-smooth muscle actin (α-SMA), and phosphorylated (phospho)-γH2AX. For CD31/ α-SMA staining, slides were loaded on a DAKO autostainer (Agilent Technologies, Dako) and serum free protein block (Agilent Technologies, Dako, catalog #X0909) was applied for 5 min. The primary antibody CD31 (BD Pharmingen, catalog #550274) was applied at 1/10 (1.56 RbIgG) for 1 h, followed by Goat Anti-Rat (BD Pharmingen, catalog #554014) for 30 min. ZSA (Invitrogen, catalog #43-4323) was applied for 30 min followed by DAB chromogen (Agilent Technologies, Dako, catalog #K3468) for 5 min. Serum free protein block (Agilent Technologies, Dako, catalog #X0909) was applied again for 5 min. α-SMA (Abcam, catalog #ab5694) was applied for 1 h at 1/125 (1.6 IgG) followed by L-AP-Rab-Poly (Powervision, catalog #PV6119) for 30 min and Fast Red (Thermo Scientific, catalog #TA-060-AL) for 10 min. Phospho-γH2AX staining was performed using the Dako EnVision+ System-HRP (Agilent Technologies, Dako, anti-Rabbit, catalog #K4011) kit with a 30 min Tris antigen retrieval step, 15 min peroxidase blocking period, an overnight primary antibody incubation (1/1000, rabbit mAb; Cell Signaling, catalog #9718S) period and 1 h secondary incubation. Whole tumor sections were captured and digitized using the ScanScope XT system (Aperio Technologies, Vista, CA). Analysis of CD31/ α-SMA staining was performed by capturing four-to-five random fields with 20× magnification for each tumor, and using Analyze PC (Analyze PC, Version 7.0, Mayo Clinic, Rochester, MN) to trace out individual vessels with a visible lumen for these fields. This analysis provided the number and lumen area (number of pixels) for each vessel in each field, where the microvessel density (MVD) represents the average number of vessels from four-to-five fields for each tumor, and the lumen area represents the average pixel area of all vessels from five fields. Quantification of phospho-γH2AX staining was performed by capturing four-to-five random fields at 20× magnification and using the Image J IHC profiler Macro [20] to calculate the percentage of positive cells.

Study design, sample sizes and statistics

For experimental studies, a total of 70 SCID mice were used to establish HPV+ (n = 33) and HPV- (n = 37) tumors subcutaneously in the leg. Tumors were allowed to grow to a mean volume of ~300 mm³ prior to being randomized into control (HPV+ n = 13; HPV- n = 14) or treatment (HPV+ n = 20; HPV- n = 23) arms. **Fig. 1** shows the experimental design for the preclinical imaging trial aimed at examining the

potential of PAI for monitoring tumor response to fRT in HPV-positive and HPV-negative PDX models of HNSCC. Animals in the treatment group received 5 daily fractions of 3 Gy for a total dose of 15 Gy (red arrows). PAI measurements (blue arrows) were obtained on day 0 (d0; before treatment), day 2 (d2; on-treatment, 2 h post 9 Gy), day 5 (d5; 24 h post completion of treatment) and day 11 (d11; 1 week post completion of therapy). B-mode US images were acquired at all PAI time points and once every three days until study completion (green arrows). A subset of animals was euthanized and tumors excised on day 2 and day 5 for immunohistochemical analysis (HPV+ PDX: control (n = 4/time point) and fRT (n = 5/time

point); HPV- PDX: control (n = 4/time point) and fRT (n = 6/time point)). All statistical analyses were performed using GraphPad Prism version 6.00 for Windows (GraphPad Software, La Jolla, CA). Changes in tumor volume were analyzed using a two-way ANOVA. Changes in tumor %sO₂ and HbT levels for either controls or fRT animals were compared using paired student's *t*-test, and when comparing controls to fRT animals at each time point unpaired student's *t*-test was used. Pearson's correlation analysis was performed for correlation plots comparing %sO₂ levels to the percent change in volume at 2 weeks following completion of treatment. For statistical modeling of tumor growth, tumor

growth rate was quantified for each mouse as the slope (indicating the absolute change/increase in tumor volume (mm³)/day) from an ordinary least squares regression of tumor volume as a function of time. Time points during tumor growth prior to radiation exposure were excluded. Unpaired two-tailed student's *t*-tests were used to compare differences in immunohistochemical parameters between control and fRT-treated samples at each time point.

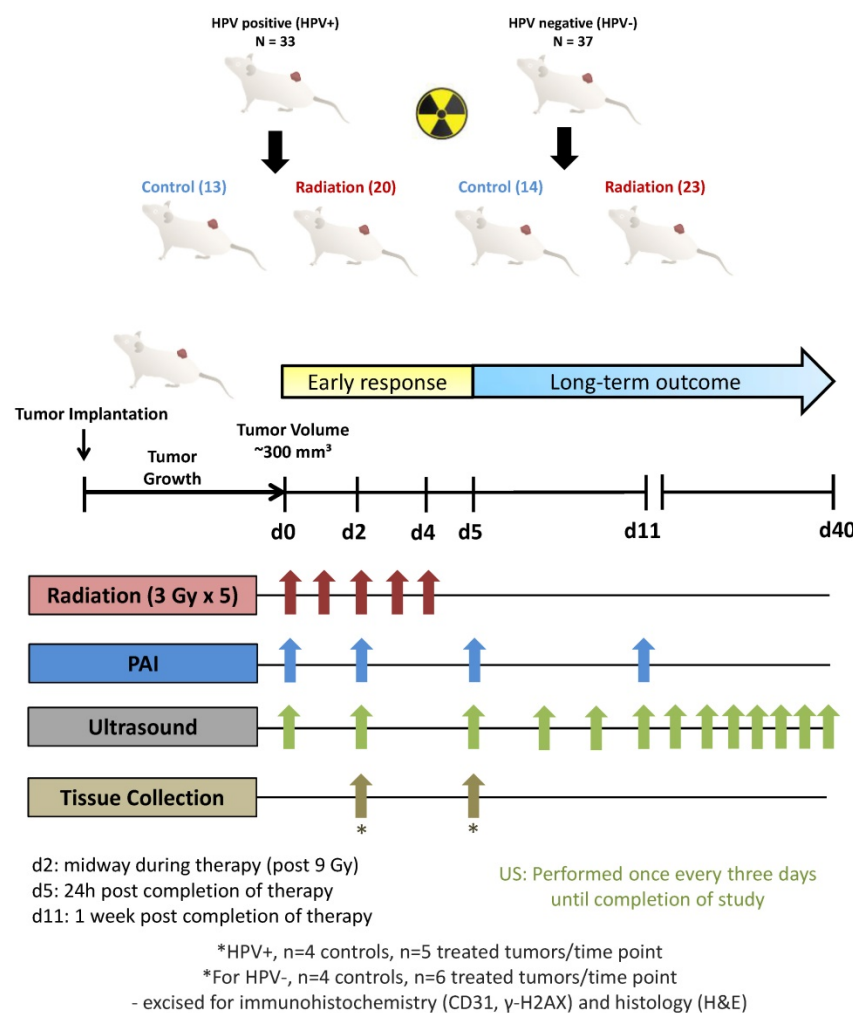


Figure 1. Study design for the preclinical imaging trial of photoacoustic imaging for monitoring RT in PDX models of head and neck cancer. A total of 70 SCID mice were used to establish HPV+ (n = 33) and HPV- (n = 37) tumors subcutaneously in the leg. Tumors were allowed to grow to ~300 mm³ prior to being randomized into control (HPV+ n = 13; HPV- n = 14) or treatment (HPV+ n = 20; HPV- n = 23) arms. Animals in the treatment group received 5 daily fractions of 3 Gy for a total dose of 15 Gy (red arrows). PAI measurements (blue arrows) were obtained on day 0 (d0; before treatment), day 2 (d2; on-treatment, post 9 Gy), day 5 (d5; 24 h post completion of treatment) and day 11 (d11; 1 week post completion of therapy). B-mode US images were acquired at all PAI time points and once every three days until study completion (green arrows). A subset of animals was euthanized and tumors excised on day 2 and day 5 for immunohistochemical analysis (HPV+ PDX: control (n = 4/time point) and fRT (n = 5/time point); HPV- PDX: control (n = 4/time point) and fRT (n = 6/time point)). Long-term treatment outcome was assessed by measuring tumor volumes up to 40 days post treatment.

Results

PAI detects early fluctuations in tumor oxygenation during and after fractionated RT prior to change in tumor volume

First, we compared tumor %sO₂ levels in control and fRT-treated tumors before, during and after fRT using PAI. PAI with co-registered US was performed on a total of 21 tumor-bearing mice (HPV- n = 11; HPV+ n = 10) that underwent fractionated RT (fRT; 3 Gy × 5). Temporal measurements of tumor %sO₂ were obtained for all 21 animals at baseline and at different times during and after fRT. Longitudinal PAI revealed distinct temporal profiles of tumor oxygenation between HPV- and HPV+ tumor xenografts. In the HPV- PDX model (Fig. 2A), untreated control tumors showed fluctuations in tumor %sO₂ during

the 12 day imaging period. These differences were not statistically significant. Serial PAI of tumors in the fRT group revealed an early increase ($p < 0.05$) in oxygen saturation from d0 to d2 during treatment (post 9 Gy) followed by a reduction on day 5 (24 h post 15 Gy). No difference was observed between control and treated tumors during this 5 day period. One week post completion of treatment (day 11), tumors in the fRT group showed a significant reduction in tumor %sO₂ compared to baseline ($p < 0.01$), d2 ($p < 0.001$) and d5 estimates ($p < 0.01$) and control tumors ($p < 0.05$) at the same time point. Intra-tumoral hemoglobin concentration (HbT) was lower ($p < 0.01$) in treated tumors compared to baseline (pre-treatment) estimates (Fig. 2B). In the HPV+ PDX model (Fig. 2D), tumor %sO₂ levels remained relatively steady during the course of treatment but were significantly lower on day 11 ($p < 0.001$ vs. d0; $p < 0.001$ vs. d2; $p < 0.01$ vs. d5). Similarly, HbT levels (Fig. 2E) showed a significant reduction at 1 week post treatment (d11) compared to baseline ($p < 0.05$) and estimates during treatment ($p < 0.001$ vs. d2; $p < 0.01$ vs. d5). We compared tumor hemodynamic changes detected by PAI in the context of changes in tumor size induced by fRT. To this end, B-mode US was utilized to obtain 3D measurements of tumor volume before, during and after treatment. In both models (Fig. 2C, F), differences in US-based tumor volumes between control and treatment groups were not significant during the early response assessment period (d0-d5). At 1 week post treatment (d11), HPV+ tumors in the fRT group showed a significant reduction in tumor volume compared to control tumors ($p < 0.01$; Fig. 2F). No difference in tumor volume was observed between control and fRT tumors in the HPV- model (Fig. 2C). These observations demonstrate the ability of PAI to monitor early changes in oxygenation of head and neck tumors prior to macroscopic changes in tumor volume.

Photoacoustic mapping of inter-tumoral heterogeneity in oxygen saturation

Next, we examined the inter-tumoral heterogeneity in oxygenation of HPV+ and HPV- PDX models of HNSCC using PAI. Fig. 3 shows dynamic changes in tumor %sO₂ measured by PAI from baseline to 24 h post completion of therapy for individual HPV- (A, B) and HPV+ (C, D) xenografts. Pseudo-colored parametric maps of %sO₂ overlaid on the B-mode US image are shown for two individual HPV- (Fig. 3A) and HPV+ (Fig. 3C) tumors at baseline (d0), post 9 Gy (d2), and 24 h post 15 Gy (d5). PAI revealed considerable inter-tumoral heterogeneity in tumor oxygenation before and during fRT in both tumor models. While some tumors showed a sustained

increase in %sO₂ throughout fRT (Fig. 3A, C, top panel), others showed an early increase post 9 Gy but subsequently decreased post 15 Gy (Fig. 3A, C, bottom panel). Corresponding bar graphs show fluctuations in %sO₂ levels of all individual tumors in HPV- (Fig. 3B) and HPV+ (Fig. 3D) xenografts that underwent fRT. Change in oxygen saturation values of individual tumors at baseline (pre-treatment; black bars), day 2 (post 9 Gy; blue bars), d5 (post 15 Gy; red bars), illustrate the temporal heterogeneity in tumor oxygenation status during the course of treatment. No correlation was observed between tumor volume and baseline estimates of tumor %sO₂.

Vascular response and fRT-induced DNA damage in HPV+ and HPV- xenografts

To gain insight into the mechanisms underlying PAI observations, a subset of animals from control and treatment groups were euthanized and tumors excised post 9 Gy (d2) and 24 h post 15 Gy (d5) for immunostaining. Tumor sections were immunostained for CD31 to assess changes in vascularity (Fig. 4) and phosphorylated γ H2AX (phospho- γ H2AX; Fig. 5) to evaluate fRT-induced DNA damage. The effect of fRT on microvessel density (MVD) and vessel lumen area was quantified from CD31-immunostained sections at each time point. In the HPV- PDX model, no difference in MVD or lumen area was observed on d2 (post 9 Gy). A significant reduction in MVD was observed on d5 (post 15 Gy; Fig. 4B) compared to control tumors (d5; $p < 0.05$). Comparative evaluation of irradiated tumors between the two time points revealed a significant reduction in MVD on d5 (compared to d2; $p < 0.01$), which was accompanied by a significant increase in lumen area (Fig. 4C). No significant change in MVD (Fig. 4E) or lumen area (Fig. 4F) was observed for HPV+ PDX at either time point.

Phospho- γ H2AX staining was performed to measure fRT-induced DNA damage in HPV+ and HPV- PDX (Fig. 5A, C). The panel of images shown in Fig. 5A represents photomicrographs of phospho- γ H2AX-stained tumor sections from control and treatment groups at both time points. A magnified image of a region within each tumor is also shown. On d2 (post 9 Gy), no difference in phospho- γ H2AX positivity was seen between control and irradiated tumors in the HPV- xenograft model (Fig. 5B). A significant increase ($p < 0.01$) in phospho- γ H2AX was observed in HPV+ PDX compared to controls (Fig. 5C). Twenty-four hours post completion of therapy (d5; post 15 Gy), irradiated sections from the HPV- PDX (Fig. 5B) and HPV+ PDX (Fig. 5C) showed a significant increase ($p < 0.01$) in phospho- γ H2AX positivity.

PAI as an early surrogate marker of radiotherapeutic efficacy in HNSCC

To determine if early changes in oxygenation detected by PAI provided information on the long-term treatment outcome, we correlated baseline (pretreatment), on-treatment (post 9 Gy), and post treatment (post 15 Gy) %sO₂ values of individual tumors with relative change in tumor volume at 2 weeks post therapy. Absolute measurements of %sO₂ obtained at the individual time points at baseline (pre-treatment), on-treatment (post 9 Gy) or after

completion of therapy did not show any correlation with tumor volume change at two weeks post therapy in both HPV- and HPV+ models (Fig. S1). Similarly, HbT measurements obtained at baseline and post treatment did not show any correlation with relative change in tumor volume (Fig. S2). Interestingly, higher HbT values on-treatment (post 9 Gy) were associated with increased tumor growth ($r = 0.7038$; $p < 0.05$) in the HPV- PDX but not in the HPV+ PDX (Fig. S2).

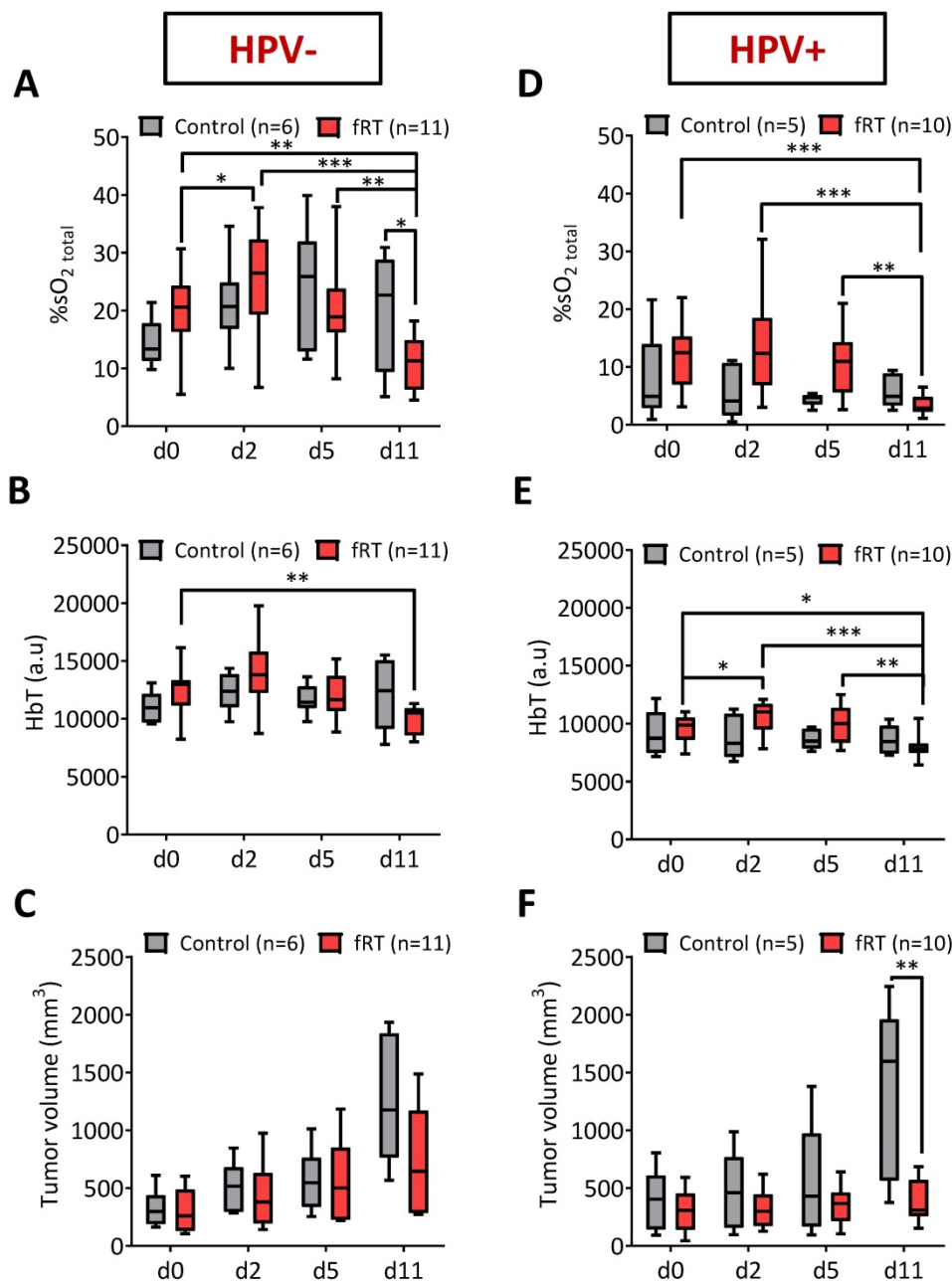


Figure 2. Photoacoustic monitoring of tumor oxygenation kinetics before, during and after fRT in head and neck cancer. Box-and-whisker plots show PAI-based measures of oxygen saturation (%sO₂) and total hemoglobin concentration (HbT) of HPV- (A, B) and HPV+ (D, E) tumors in the control and fRT groups at baseline (d0), post 9 Gy (d2), post 15 Gy (d5), and one week (d11) following completion of fRT. (C, F) Grouped tumor volumes of animals in control (n = 6) and fRT groups (n = 11) at baseline (d0), post 9 Gy (d2), post 15 Gy (d5), and one week (d11) following completion of fRT. Changes in PAI parameters were observed prior to visible changes in tumor volume in both tumor models. *P<0.05, **P<0.01, ***P<0.001.

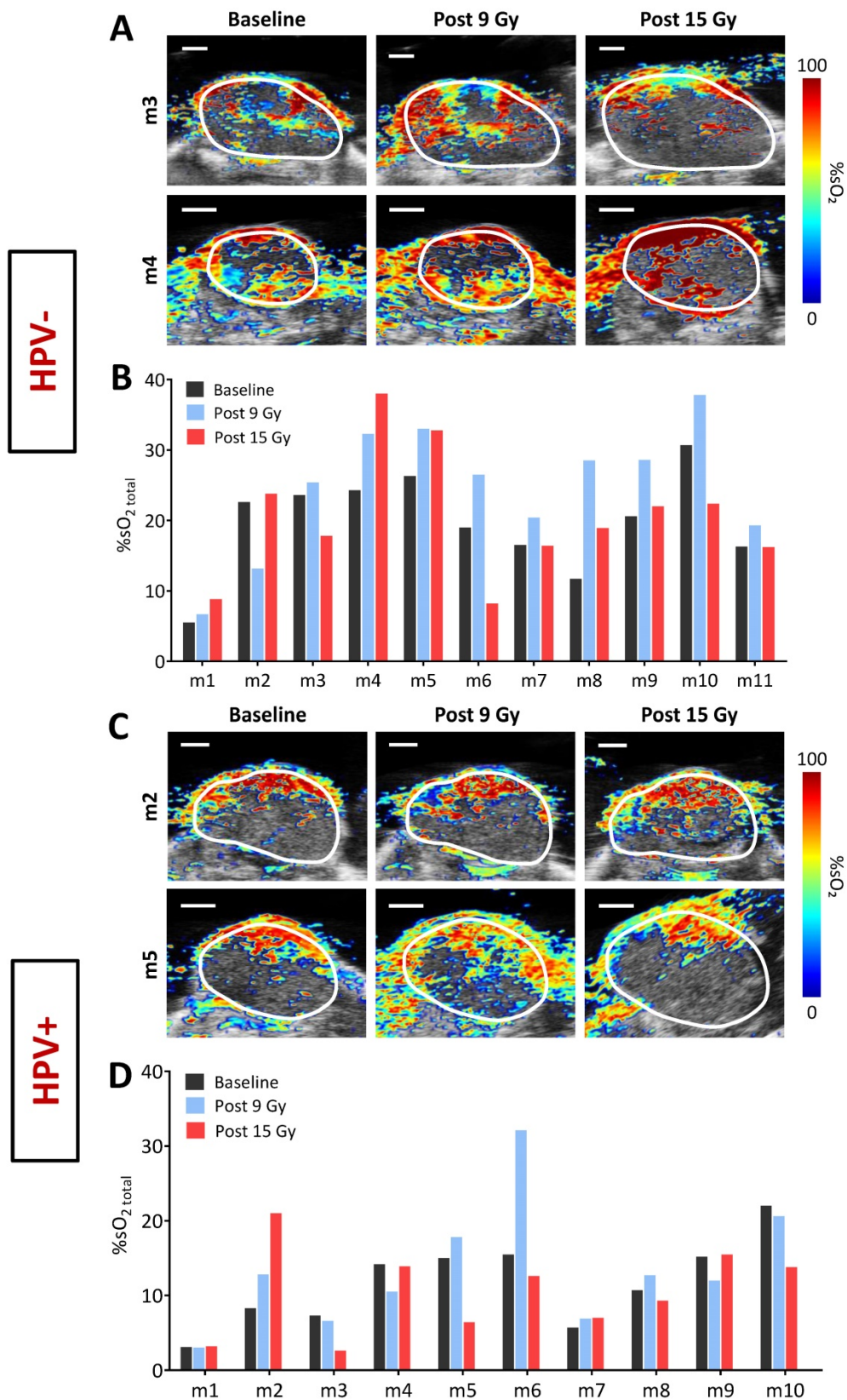


Figure 3. Optoacoustic mapping of fluctuations in tumor oxygenation before, during and immediately following completion of fRT in head and neck cancer. Pseudo-colored tumor %sO₂ maps of individual HPV+ and HPV- tumors overlaid on their B-mode ultrasound images at baseline (d0), post 9 Gy (d2), and post 15 Gy (d5) are shown in **A** and **C**, respectively (scale bars represent 2 mm in length). Some tumors showed a sustained increase in %sO₂ throughout fRT (top), while others increased post 9 Gy but went down post 15 Gy (bottom). Corresponding bar graphs show fluctuations in %sO₂ levels of individual tumors in HPV- (**B**) and HPV+ (**D**) xenografts that underwent fRT.

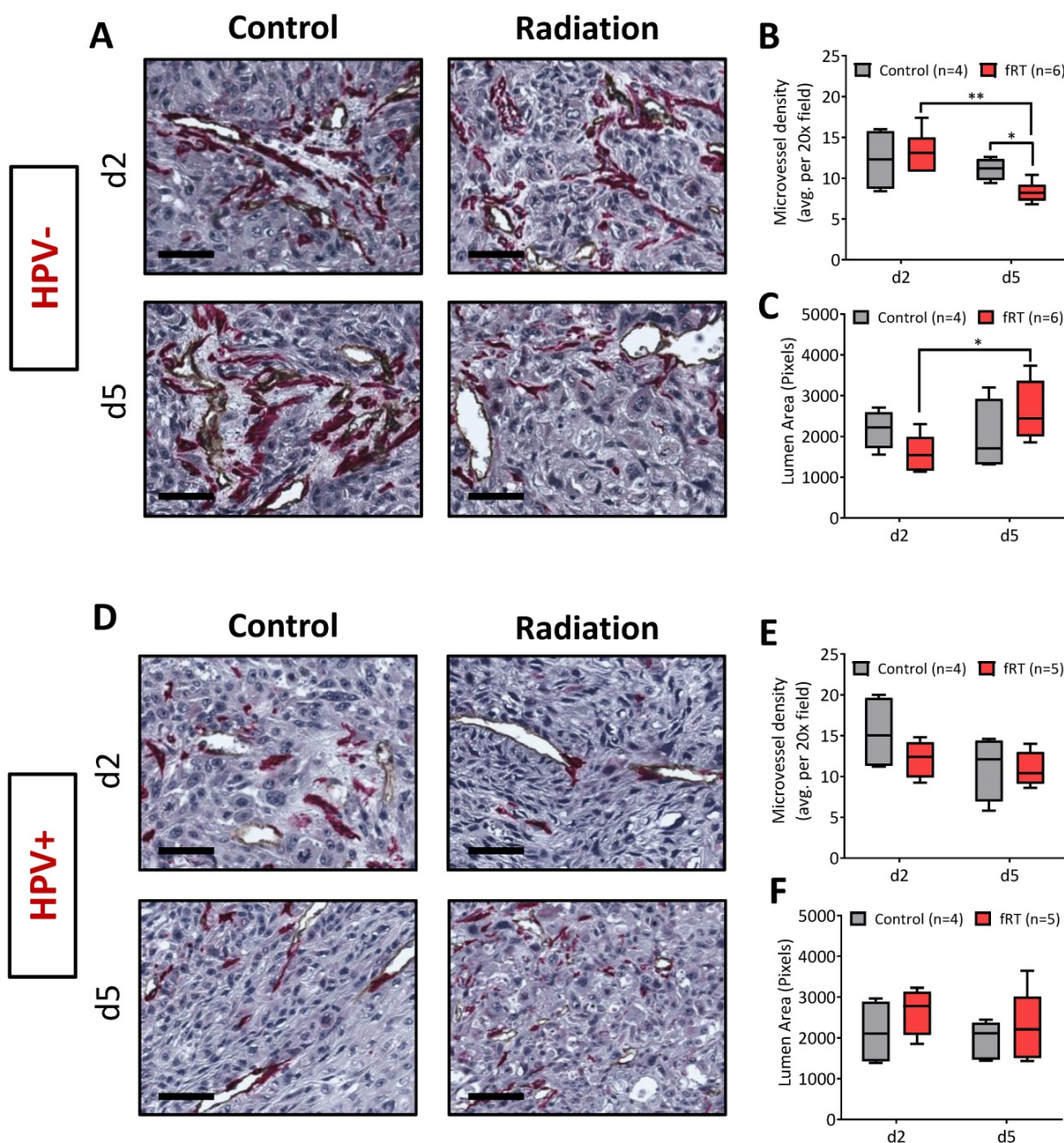


Figure 4. Vascular response of HPV+ and HPV- xenografts to fractionated RT. Photomicrographs of CD31/ α -SMA-stained tumor sections of HPV- (A) and HPV+ (D) HNSCC xenografts from both control and treatment groups (scale bars represent 50 μ m in length). Tumors were excised post 9 Gy (d2) and 24 hours post 15 Gy (d5) for immunohistochemical analysis (HPV+ PDX: control (n = 4/time point) and fractionated RT (n = 5/time point); HPV- PDX: control (n = 4/time point) and fractionated RT (n = 6/time point)). Microvessel density (B, E) and vessel lumen area (C, F) were quantified from CD31-immunostained sections at each time point. *P<0.05, **P<0.01.

Next, we examined the relationship between change in %sO₂ during and immediately after treatment with tumor control at two weeks post therapy (Fig. 6). Correlation plots between percent change in volume at 2 weeks post treatment with change in %sO₂ and HbT levels from baseline to post 9 Gy, baseline to post 15 Gy, and post 9 Gy to post 15 Gy for the HPV- PDX (Fig. 6A-F) and the HPV+PDX (Fig. 6G-L) are shown. In the HPV- PDX model, increases in %sO₂ levels during treatment (baseline to post 15 Gy; Fig. 6B) negatively correlated with better tumor control (r = -0.6421; p<0.05). Tumors that showed an

increase in %sO₂ levels during the second half of fRT (post 9 Gy to 15 Gy; Fig. 6C) showed greater tumor growth inhibition (r = -0.7969, p<0.01) compared to tumors that showed minimal change or reduction in %sO₂ levels. A similar relationship was seen between change in HbT levels and tumor control, with tumors with higher levels of HbT during treatment exhibiting a more favorable response to therapy (Fig. 6E, F). Interestingly, no such correlation was seen between PAI parameters of %sO₂ and HbT with tumor control in the HPV+ PDX model (Fig. 6G-L).

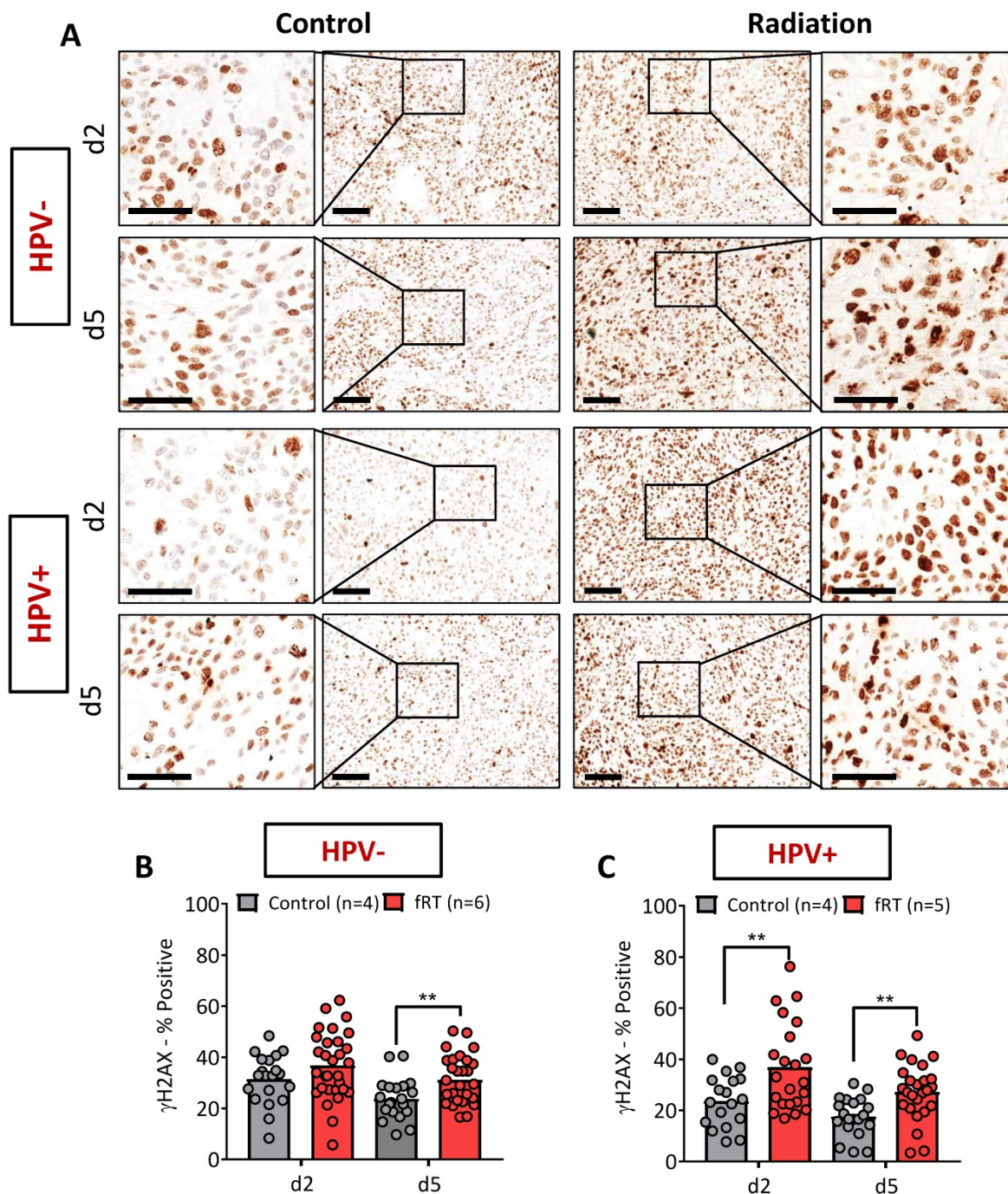


Figure 5. Immunohistochemical assessment of fRT-induced DNA damage in HPV- and HPV+ xenografts. (A) Photomicrographs of phospho-γH2AX-stained tumor sections from control and treatment groups at both time points (scale bars represent 100 μm in length). A magnified image of a region within each tumor is also shown (scale bars represent 50 μm in length). Bar graphs show quantitative estimates of phospho-γH2AX positivity in HPV- (B) and HPV+ (C) xenografts. Bars represent mean values for control (gray) and irradiated tumors (red) while the circles represent individual 20× fields within a tumor. Four to five fields were evaluated for each tumor (n = 4-6 per group/time point). **P<0.01.

To be useful as a surrogate measure of RT efficacy, PAI measures should enhance the accuracy of a response algorithm that already accounts for HPV status. To assess the prognostic utility of PAI parameters, we performed statistical modeling of temporal PAI read-outs (%sO₂ and HbT) of all tumors (in both control and fRT groups). A linear mixed

model was used to model hemodynamic changes measured by PAI in relation to treatment outcomes measured by tumor growth rate. Absolute and relative measurements of %sO₂ and HbT were modeled to examine the effects of HPV, radiation and all 2nd and 3rd order interactions. Baseline tumor volume measurements were not included as a

covariate in the models as exploratory analysis did not show any evidence of association with either growth rate or HPV/radiation factors (Fig. S3). As shown in Table S1, modeling tumor growth kinetics and temporal PAI datasets revealed statistically significant effects for relative change in %sO₂ measurements from d0-d2, d0-d5 and d0-d12 (p<0.01) and for HbT values on d5 (p<0.05).

Long-term response of HPV+ and HPV-xenografts to fRT mimics clinical behavior

Finally, we examined the long-term response of the HPV- and HPV+ tumors to fRT. US-based tumor volume measurements were utilized to calculate tumor growth rates of individual tumors (Fig. S4 and Fig. S5). In control animals (Fig. S6), the distribution of growth rates (Table 1) showed faster growth rates in the HPV- PDX model (94.39 ± 34.3 mm³/day) compared to HPV+ PDX (78.61 ± 36.4 mm³/day). A differential response to fRT was seen between HPV- (Fig. 7A) and HPV+ tumors (Fig. 7B and Fig. S6) with a significantly (p=0.0187) greater tumor growth rate inhibition (Table 2) seen in the HPV+ PDX model (2.95 ± 8.3 mm³/day) compared to the HPV- PDX model (26.99 ± 13.23 mm³/day). Compared to untreated controls, fRT resulted in a significant (p<0.0001) reduction in tumor growth rate in HPV- and HPV+ xenografts (Table 2).

Table 1. Grouped growth rates for control and fRT treated HPV+ and HPV- PDX.

		HPV-		
Group	N	Mean	Std	Median
Control	6	94.39	34.37	97.73
Radiation	11	26.99	34.37	30.13
		HPV+		
Group	N	Mean	Std	Median
Control	5	78.61	36.42	91.49
Radiation	10	2.95	8.35	2.47

Table 2. Least squares means analysis comparing tumor type and treatment groups.

Least Squares Means				
Group	Tumor Type	Growth rate	LSMEAN #	
Control	HPV-	94.39	1	
Control	HPV+	78.60	2	
Radiation	HPV-	26.99	3	
Radiation	HPV+	2.95	4	
Least Squares Means for effect radn*tumor type				
	1	2	3	4
1		0.2468	<0.0001	<0.0001
2	0.2468		<0.0002	<0.0001
3	<0.0001	<0.0002		0.0187
4	<0.0001	<0.0001	0.0187	

Discussion

Given the impact of oxygenation on the efficacy of radiotherapy, there has been a long-standing

interest in the development of non-invasive methods to image the dynamic changes in oxygenation occurring within the tumor microenvironment [21]. PET using 18F-FAZA has been shown to correlate/predict outcome following RT [22, 23], but PET is expensive and requires the use of radioisotopes that limit frequent and repetitive use. The optimal timing for PET, CT or MRI-based assessment of hypoxia is also not clear [24]. In this regard, PAI offers a cost-effective, high-throughput alternative to non-invasively map tumor oxygenation *in vivo*. PAI combines the high contrast and specificity of optical imaging techniques with the clinically relevant imaging depths achievable with US [13, 14]. Consequently, PAI-based assessment of tumor oxygenation could be useful for clinical assessment of hypoxia. In this regard, we have previously validated PAI measures of %sO₂ with direct measurements of pO₂, blood oxygenation level-dependent magnetic resonance imaging [25] and oxygen-enhanced MRI [26] in tissue-mimicking phantoms and in tumor models. Published studies by others have also demonstrated a good correlation between PAI read-outs and contrast-enhanced ultrasound (CE-US)-based estimates of tumor vascular parameters [27, 28]. Building on this earlier work, in the present study, we (i) investigated temporal fluctuations in tumor sO₂ in HPV+ and HPV- head and neck carcinoma xenografts following a clinically-relevant fractionated RT regimen, (ii) evaluated the short-term and long-term response of HPV+ and HPV- xenografts to fractionated RT using PAI with co-registered US, and, (iii) performed statistical modeling of PAI-based measurements of sO₂ obtained at baseline, during and after fractionated RT with long-term response of individual mice to determine the ability of PAI to serve as a 'biomarker' of RT efficacy. The short acquisition times and the lack of ionizing radiation or radioactive isotopes enabled serial imaging before, during and after fRT. PAI revealed considerable intra- and inter-tumoral heterogeneity in sO₂ prior to treatment. PAI-based changes in sO₂ were detected within a few days after the start of fRT prior to detectable change in tumor volume, highlighting the potential of PAI to serve as an early biomarker of treatment response or resistance. Our observations suggest that vascular and cellular response to radiation [29] results in fluctuations in oxygenation that precede changes in macroscopic tumor volume.

Comparative assessment of the two models showed faster growth rates in the HPV- tumors than HPV+ tumors. A differential response to RT was also observed between HPV+ and HPV- tumors. Multiple trials have demonstrated improved outcomes in HPV+ oropharyngeal cancer patients compared to

their HPV- counterparts [16, 17]. Consistent with the favorable outcome seen in patients with HPV+ HNSCC, we observed superior tumor control in the HPV+ PDX model compared to the HPV- PDX model. We observed statistically significant associations between PAI-based measures of %sO₂ and HbT with treatment outcomes. In the HPV- model, increases in tumor oxygenation throughout fRT were associated with a favorable response to treatment. The strongest correlation was observed between changes in tumor

%sO₂ from post 9 Gy to post 15 Gy with tumor growth inhibition. This indicates that tumors that maintained high %sO₂ levels in the second half of fRT responded the best. Tumors that showed an increase in %sO₂ during the first half of treatment but subsequently decreased were not as responsive. Collectively, our findings highlight the value of temporal PAI measurements of oxygenation kinetics in monitoring and potentially predicting RT efficacy.

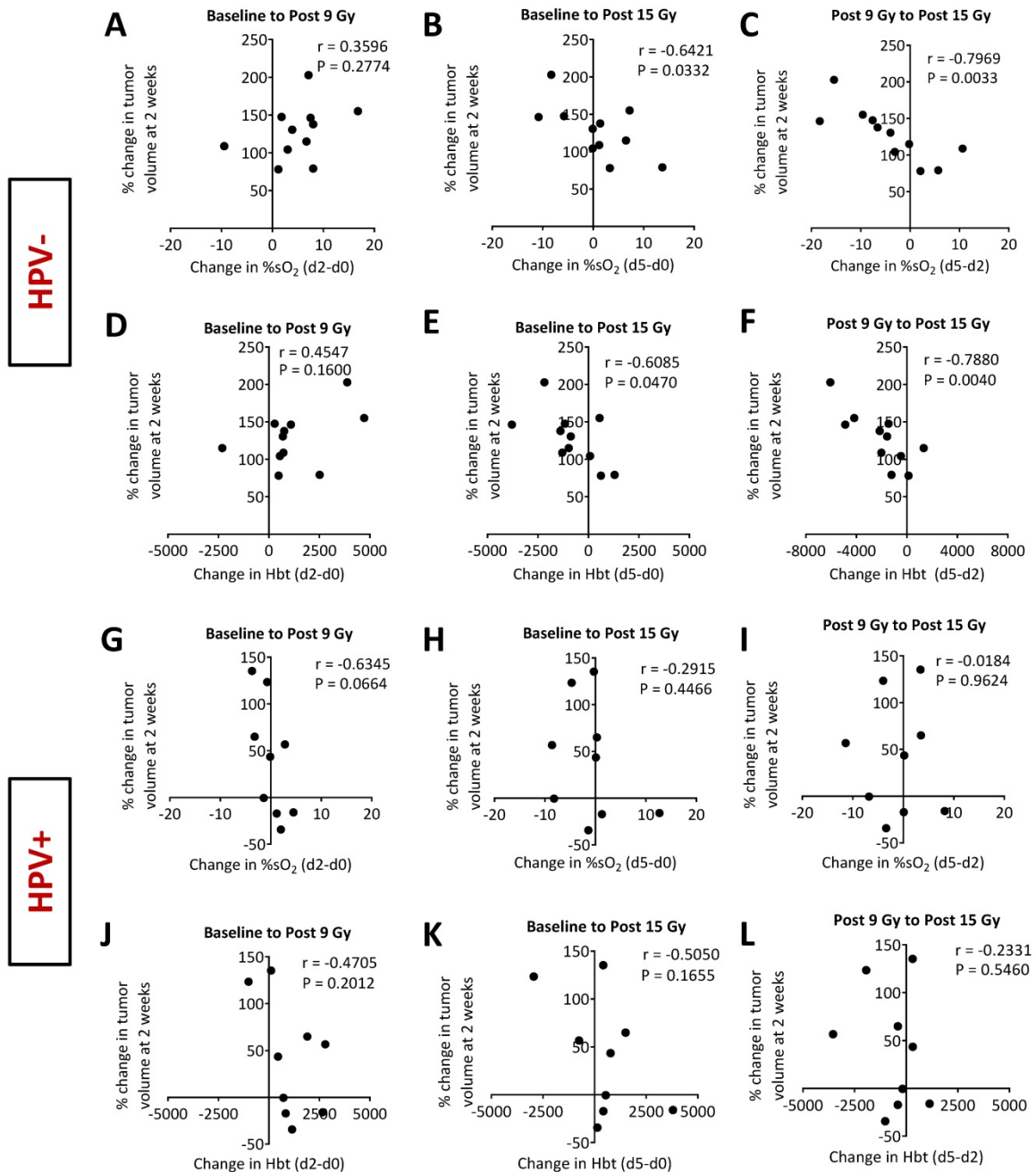


Figure 6. Photoacoustic imaging as an early surrogate measure of fRT efficacy in head and neck cancer. Correlation plots comparing percent change in volume at 2 weeks following completion of fRT with change in %sO₂ (A-C for HPV- and G-I for HPV+) and HbT (D-F for HPV- and J-L for HPV+) from baseline to post 9 Gy, baseline to post 15 Gy, and post 9 Gy to post 15 Gy in models of HNSCC. Increase in %sO₂ and HbT for HPV- tumors during fRT was associated with a favorable treatment outcome.

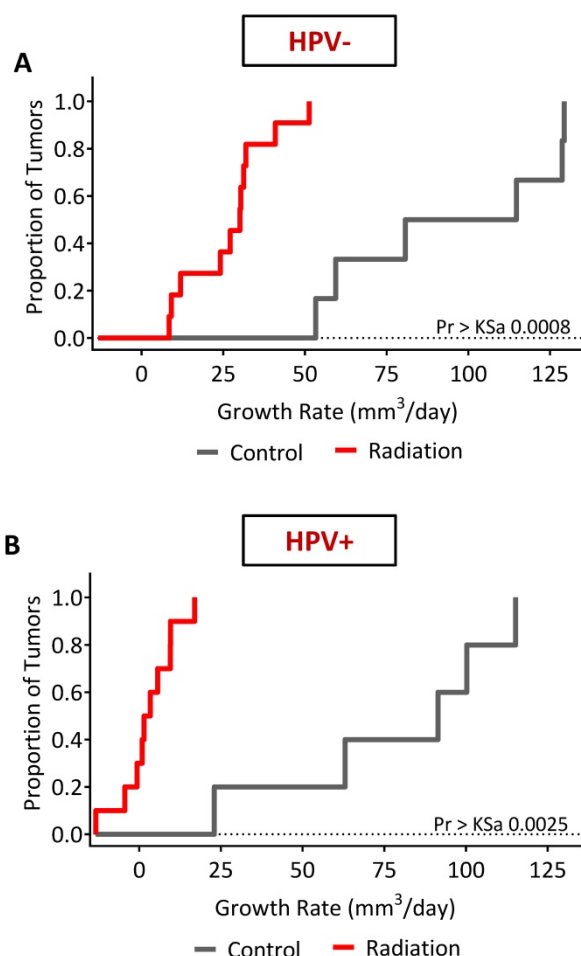


Figure 7. Long-term treatment outcome following fRT in HPV+ and HPV- PDX models of HNSCC. The effects of radiation on tumor growth rate in HPV- (A) and HPV+ (B) xenografts were estimated using an ANOVA model. The model was specified with main effects for radiation, tumor type and the interaction. Radiation therapy resulted in a significant reduction in tumor growth rate compared to control animals in both models. Tumor response to radiation was much more pronounced in the HPV+ PDX model compared to the HPV- tumors.

Our observations have some precedence in the literature [30-32]. Hoff et al., have previously demonstrated the prognostic utility of Hb in head and neck tumor response to radiotherapy [30]. Specifically, patients with high pretreatment Hb levels had a significantly better probability of locoregional control, disease-specific survival and overall survival compared to patients with low Hb levels. Similar observations have also been reported by McCloskey and colleagues [31]. Using diffuse reflectance spectroscopy, Hu et al., have recently shown that rate of oxygenation increase was dependent on the radiation dose and correlated with recurrence in HPV-negative FaDu xenografts [32]. Specifically, the authors observed that locally recurrent tumors showed slower increases in oxygenation after RT compared to tumors that were locally controlled with RT. Recently, Dong et al. [33] validated these findings in HNSCC patients, showing

that responsive tumors experienced increased sO₂ levels throughout treatment. They also found that HPV+ tumors experienced greater increases in sO₂ than the HPV- tumors. While the mechanisms that contribute to the observed changes in oxygenation are unclear, they are likely to be multi-factorial. Sustained increase in %sO₂ throughout treatment could be associated with elevated tumor cell apoptosis and a reduction in the number of viable tumor cells, lowering the metabolic demand of the tumor. It is also possible that this reduction in cell number could relieve the interstitial fluid pressure levels within the tumor, increasing tumor blood flow levels [34].

To investigate the possible mechanisms behind the observed fluctuations in sO₂ in our experimental models, we performed correlative immunostaining of tumor sections for markers of vascularity (CD31) and DNA damage (phospho-γH2AX). CD31 analysis revealed a significant reduction in MVD and increased lumen area post 15 Gy in the HPV-xenograft model, although no change was observed in HPV+ PDX. This observation is consistent with a previous study in which radiation-induced re-oxygenation in murine SCCVII carcinomas was associated with an overall reduction in tumor MVD and increased vessel perfusion [35, 36]. Although a similar pattern of phospho-γH2AX foci formation was seen in HPV+ and HPV- tumors following fRT, we observed a difference in the kinetics of DNA damage between the two tumor models. A significant accumulation of phospho-γH2AX foci was observed in the HPV+ model early on during treatment (post 9 Gy), which persisted after completion of fRT, indicating increased susceptibility of the HPV+ xenograft to fRT-induced DNA double strand breaks. This observation is supported by a previous study by Taneja et al., in which radiosensitive cell lines and xenografts were shown to retain γH2AX for a greater duration compared to radioresistant cells [37].

Our findings have clinical implications for imaging and treatment of HNSCC. RT is a major component of the treatment paradigm for HNSCC patients and improvements in treatment planning methods and radiation delivery schemes have helped increase its therapeutic benefit. However, not all patients respond in the same manner and tumor recurrence continues to remain a clinical challenge. Early insight into treatment outcome can therefore be of immense value, particularly in patients with non-responsive tumors. As such, there is a significant clinical need in radiation oncology for an inexpensive and non-radioactive imaging modality that can provide prognostic information. In this regard, our results demonstrate that PAI-based estimates of oxygen saturation could potentially serve as an

indicator of therapeutic failure in HNSCC. Early prediction of treatment failure would enable patients to forgo toxic, ineffective therapy and opt for potentially efficacious therapy or surgery. While the application of PAI for tumor imaging is an area of active preclinical and clinical investigation [38–41], a majority of these studies have focused on examining the diagnostic potential of PAI. The results of the present study add to the limited literature on the prognostic utility of PAI based on endogenous contrast [42–44]. Although limited in number, these studies have shown that the utility of PAI-based tumor oxygenation measurements can be applied for monitoring treatment response to targeted cancer therapies [42], photodynamic therapy [43], and photothermal therapy [44]. Furthermore, clinical studies evaluating the potential of hypoxia-modifying therapies conducted in non-selected patients have been disappointing [45]. In this regard, tumor hypoxia mapping using PAI could enable selection of tumors (patients) who would benefit from hypoxia-modifying therapy. Our results point to early changes in oxygenation occurring during the delivery of initial radiation fractions influencing treatment outcome. It would therefore be interesting to evaluate if PAI-based hypoxia assessment early-on during the course of therapy can help select tumors (patients) that would benefit from hypoxia-modifying therapies or receive radiation dose de-escalation without compromising efficacy. Conversely, one could escalate the radiation dose to hypoxic regions identified on PAI examination. We have begun addressing some of these questions in our laboratory and will report on our findings in the future.

While our results support the clinical development of PAI as a biomarker of radiation response in HNSCC, the limitations of our model system and study design warrant consideration and caution while interpreting our observations. First, PDX models are useful tools to study human cancer biology in an experimental setting. The scope of these models is limited by the need for immunodeficient hosts. Despite the absence of the immune components, the observed differential response between the p16+ and p16- PDX to fRT is encouraging and consistent with the superior response of HPV+ human HNSCC to standard-of-care treatment compared to HPV-counterparts. Second, we examined one PDX model of each type (HPV+ and HPV-) with tumors established in the subcutaneous (ectopic) location. Investigation across a panel of PDX models (“Avatars”) would better recapitulate the heterogeneity in the patient population.

In summary, we have shown that PAI can be used for frequent and repeated assessment of head

and neck tumors before the start of therapy, on-treatment and following completion of therapy. Our findings illustrate the utility of PAI as a label-free, non-invasive, cost-effective method for serial monitoring of tumor oxygenation following RT. As such, RT remains one of the most economical and effective treatments for cancer. Our findings are therefore relevant to the clinical utility of PAI not limited to head and neck cancers but potentially other solid tumors for which fractionated RT is routinely utilized as standard-of-care. Temporal measures of tumor oxygenation measured by PAI could potentially assist in clinical decisions regarding aggressive intervention, treatment de-intensification or use of hypoxia-modifying therapies.

Abbreviations

%sO₂: Oxygen Saturation; fRT: Fractionated Radiation Therapy; HbT: Hemoglobin Concentration (a.u.); HNSCC: Head and Neck Squamous Cell Carcinoma; HPV-: Human Papilloma Virus Negative; HPV+: Human Papilloma Virus Positive; PAI: Photoacoustic Imaging; PDX: Patient Derived Xenograft; RPCI: Roswell Park Cancer Institute; RT: Radiation Therapy; SCC: Squamous Cell Carcinoma; SCID: Severe Combined Immunodeficient; US: Ultrasound; α -SMA: Alpha-Smooth Muscle Actin.

Supplementary Material

Supplementary figures and tables.

<http://www.thno.org/v08p2064s1.pdf>

Acknowledgments

The authors gratefully acknowledge the patients who kindly provided tumor specimens used to generate the PDX model described in the study. The authors would like to thank Ms. Stephanie Denzler for assistance with *in vivo* studies and staff members of the Laboratory Animal Shared Resource, Translational Imaging Shared Resource and the Pathology Resource Shared Network at RPCI. This work was supported by grants from the NIH/NCI R01CA204636, NIH/NIDCR R01DE024595, NIH/OD S10OD010393 and the Alliance Foundation of Western New York (all to M.S), and utilized shared resources supported the NCI Cancer Center Support Grant P30CA016156 (Johnson, CS).

Author contributions

M.S., and L.J.R. conceived and designed experiments with input from A.K.S., and A.M. L.J.R. performed all studies and analyzed the data; L.J.R., A.M., A.K.S., and M.S. interpreted the data. A.M. performed statistical analysis of the data. L.J.R., and M.S. wrote the manuscript with feedback from other

authors. All the authors reviewed and approved the final version of the manuscript. M.S. provided administrative, technical or material support supervised and coordinated all aspects of the work.

Competing interests

A portion of this work was presented at the 2016 World Molecular Imaging Congress, held in New York. L.J. R was a recipient of a Vevo Travel Award from FujiFilm VisualSonics that provide partial support for his attendance at the meeting. The remaining authors do not have any conflicts of interest to disclose. The funding sponsors had no role in the design of the study, collection, analyses, or interpretation of data, writing of the manuscript, and in the decision to publish the results.

References

- Argiris A, Karamouzis MV, Raben D, Ferris RL. Head and neck cancer. *The Lancet*. 2008; 371(9625): 1695-709.
- Walden MJ, Aygun N. Head and neck cancer. *Semin Roentgenol*. 2013; 48(1): 75-86.
- Vokes EE, Weichselbaum RR, Lippman SM, Hong WK. Head and neck cancer. *N Engl J Med*. 1993; 328(3): 184-94.
- Cognetti DM, Weber RS, Lai SY. Head and neck cancer: An evolving treatment paradigm. *Cancer*. 2008; 113(7 Suppl): 1911-32.
- Pignon JP, Bourhis J, Domenge C, Designe L. Chemotherapy added to locoregional treatment for head and neck squamous-cell carcinoma: Three meta-analyses of updated individual data. MACH-NC collaborative group. meta-analysis of chemotherapy on head and neck cancer. *Lancet*. 2000; 355(9208): 949-55.
- Joiner MC, Van der Kogel A, et al. *Basic clinical radiobiology*. 4th ed. CRC Press. 2009.
- Melillo G, et al. *Hypoxia and Cancer; Biological Implications and Therapeutic Opportunities*. 1st ed. Humana Press; 2014.
- Moulder JE, Rockwell S. Hypoxic fractions of solid tumors: Experimental techniques, methods of analysis, and a survey of existing data. *Int J Radiat Oncol Biol Phys*. 1984; 10(5): 695-712.
- Rockwell S, Dobrucki IT, Kim EY, Marrison ST, Vu VT. Hypoxia and radiation therapy: Past history, ongoing research, and future promise. *Curr Mol Med*. 2009; 9(4): 442-58.
- Klimowicz AC, Bose P, Petrillo SK, Magliocco AM, Dort JC, Brockton NT. The prognostic impact of a combined carbonic anhydrase IX and Ki67 signature in oral squamous cell carcinoma. *Br J Cancer*. 2013; 109(7): 1859-66.
- Toustrup K, Sorensen BS, Nordmark M, Busk M, Wiuf C, Alsner J, Overgaard J. Development of a hypoxia gene expression classifier with predictive impact for hypoxic modification of radiotherapy in head and neck cancer. *Cancer Res*. 2011; 71(17): 5293-31.
- Le QT, Kovacs MS, Dorie MJ, Koong A, Terris DJ, Pinto HA, Goffinet DR, Nowels K, Bloch D, Brown JM. Comparison of the comet assay and the oxygen microelectrode for measuring tumor oxygenation in head-and-neck cancer patients. *Int J Radiat Oncol Biol Phys*. 2003; 56(2): 375-83.
- Kruger RA, Liu P, Fang YR, Appledorn CR. Photoacoustic ultrasound (PAUS)--reconstruction tomography. *Med Phys*. 1995; 22(10): 1605-9.
- Xu M, Wang LV. Photoacoustic imaging in biomedicine. *Rev Sci Instrum*. 2006; 77(4): 041101.
- Kreimer AR, Clifford GM, Boyle P, Franceschi S. Human papillomavirus types in head and neck squamous cell carcinomas worldwide: A systematic review. *Cancer Epidemiol Biomarkers Prev*. 2005; 14(2): 467-75.
- Marur S, D'Souza G, Westra WH, Forastiere AA. HPV-associated head and neck cancer: A virus-related cancer epidemic. *Lancet Oncol*. 2010; 11(8): 781-9.
- Fakhry C, Westra WH, Li S, Cmelak A, Ridge JA, Pinto H, Forastiere A, Gillison ML. Improved survival of patients with human papillomavirus-positive head and neck squamous cell carcinoma in a prospective clinical trial. *J Natl Cancer Inst*. 2008; 100(4): 261-9.
- Seshadri M, Merzianu M, Tang H, Rigual NR, Sullivan M, Loree TR, Popat SR, Repasky EA, Hylander BL. Establishment and characterization of patient tumor-derived head and neck squamous cell carcinoma xenografts. *Cancer Biol Ther*. 2009; 8(23): 2275-83.
- Needles A, Heinmiller A, Sun J, Theodoropoulos C, Bates D, Hirson D, Yin M, Foster FS. Development and initial application of a fully integrated photoacoustic micro-ultrasound system. *IEEE Trans Ultrason Ferroelectr Freq Control*. 2013; 60(5): 888-97.
- Schneider CA, Rasband WS, Eliceiri KW. NIH Image to ImageJ: 25 years of image analysis. *Nat Methods*. 2012; 9(7): 671-5.
- Horsman MR, Mortensen LS, Petersen JB, Busk M, Overgaard J. Imaging hypoxia to improve radiotherapy outcome. *Nat Rev Clin Oncol*. 2012; 9(12): 674-87.
- Servagi-Vernat S, Differding S, Hanin FX, Labar D, Bol A, Lee JA, Gregoire V. A prospective clinical study of (1)(8)F-FAZA PET-CT hypoxia imaging in head and neck squamous cell carcinoma before and during radiation therapy. *Eur J Nucl Med Mol Imaging*. 2014; 41(8): 1544-52.
- Thorwarth D, Eschmann SM, Holzner F, Paulsen F, Alber M. Combined uptake of [18F]FDG and [18F]FMISO correlates with radiation therapy outcome in head-and-neck cancer patients. *Radiother Oncol*. 2006; 80(2): 151-6.
- Bhatnagar P, Subesinghe M, Patel C, Prestwich R, Scarsbrook AF. Functional imaging for radiation treatment planning, response assessment, and adaptive therapy in head and neck cancer. *Radiographics*. 2013; 33(7): 1909-29.
- Rich LJ, Seshadri M. Photoacoustic imaging of vascular hemodynamics: Validation with blood oxygenation level-dependent MR imaging. *Radiology*. 2015; 275(1): 110-8.
- Rich LJ, Seshadri M. Photoacoustic monitoring of tumor and normal tissue response to radiation. *Sci Rep*. 2016; 6: e21237.
- Eisenbrey JR, Merton DA, Marshall A, Liu JB, Fox TB, Sridharan A, Forsberg F. Comparison of photoacoustically derived hemoglobin and oxygenation measurements with contrast-enhanced ultrasound estimated vascularity and immunohistochemical staining in a breast cancer model. *Ultrasound Imaging*. 2015; 37(1): 42-52.
- Bar-Zion A, Yin M, Adam D, Foster FS. Functional Flow Patterns and Static Blood Pooling in Tumors Revealed by Combined Contrast-Enhanced Ultrasound and Photoacoustic Imaging. *Cancer Res*. 2016; 76(15): 4320-31.
- Lyng H, Sundfor K, Rofstad EK. Changes in tumor oxygen tension during radiotherapy of uterine cervical cancer: Relationships to changes in vascular density, cell density, and frequency of mitosis and apoptosis. *Int J Radiat Oncol Biol Phys*. 2000; 46(4): 935-46.
- Hoff CM, Hansen HS, Overgaard M, Grau C, Johansen J, Bentzen J, Overgaard J. The importance of haemoglobin level and effect of transfusion in HNSCC patients treated with radiotherapy--results from the randomized DAHANCA 5 study. *Radiother Oncol*. 2011; 98(1): 28-33.
- McCloskey SA, Jaggernauth W, Rigual NR, Hicks WL Jr, Popat SR, Sullivan M, Mashtare TL Jr, Khan MK, Loree TR, Singh AK. Radiation treatment interruptions greater than one week and low hemoglobin levels (12 g/dL) are predictors of local regional failure after definitive concurrent chemotherapy and intensity-modulated radiation therapy for squamous cell carcinoma of the head and neck. *Am J Clin Oncol*. 2009; 32(6): 587-91.
- Hu F, Vishwanath K, Salama JK, Erkanli A, Peterson B, Oleson JR, Lee WT, Brizel DM, Ramanujam N, Dewhirst MW. Oxygen and perfusion kinetics in response to fractionated radiation therapy in FaDu head and neck cancer xenografts are related to treatment outcome. *Int J Radiat Oncol Biol Phys*. 2016; 96(2): 462-9.
- Dong L, Kudrimoti M, Irwin D, Chen L, Kumar S, Shang Y, Huang C, Johnson EL, Stevens SD, Shelton BJ, Yu G. Diffuse optical measurements of head and neck tumor hemodynamics for early prediction of chemoradiation therapy outcomes. *J Biomed Opt*. 2016; 21(8): 85004.
- Roh HD, Boucher Y, Kalnicki S, Buchsbaum R, Bloomer WD, Jain RK. Interstitial hypertension in carcinoma of uterine cervix in patients: Possible correlation with tumor oxygenation and radiation response. *Cancer Res*. 1991; 51(24): 6695-8.
- Olive PL. Radiation-induced reoxygenation in the SCCVII murine tumour: Evidence for a decrease in oxygen consumption and an increase in tumour perfusion. *Radiother Oncol*. 1994; 32(1): 37-46.
- Crookart N, Jordan BF, Baudalet C, Ansiaux R, Sonveaux P, Gregoire V, Beghein N, DeWever J, Bouzin C, Feron O, Gallez B. Early reoxygenation in tumors after irradiation: Determining factors and consequences for radiotherapy regimens using daily multiple fractions. *Int J Radiat Oncol Biol Phys*. 2005; 63(3): 901-10.
- Taneja N, Davis M, Choy JS, Beckett MA, Singh R, Kron SJ, Weichselbaum RR. Histone H2AX phosphorylation as a predictor of radiosensitivity and target for radiotherapy. *J Biol Chem*. 2004; 279(3): 2273-80.

38. Valluru KS, Wilson KE, Willmann JK. Photoacoustic imaging in oncology: Translational preclinical and early clinical experience. *Radiology*. 2016; 280(2): 332-49.
39. Beard P. Biomedical photoacoustic imaging. *Interface Focus*. 2011; 1(4): 602-31.
40. Dogra VS, Chinni BK, Valluru KS, Moalem J, Giampoli EJ, Evans K, Rao NA. Preliminary results of ex vivo multispectral photoacoustic imaging in the management of thyroid cancer. *AJR Am J Roentgenol*. 2014; 202(6): W552-8.
41. Mallidi S, Luke GP, Emelianov S. Photoacoustic imaging in cancer detection, diagnosis, and treatment guidance. *Trends Biotechnol*, 2011; 29(5): 213-221.
42. Lee S, Kim JH, Lee JH, Lee JH, Han JK. Non-invasive monitoring of the therapeutic response in sorafenib-treated hepatocellular carcinoma based on photoacoustic imaging. *European radiology*. 2018; 28(1): 372-381.
43. Mallidi S, Watanabe K, Timmerman D, Schoenfeld D, Hasan T. Prediction of tumor recurrence and therapy monitoring using ultrasound-guided photoacoustic imaging. *Theranostics*. 2015; 5(3): 289-301.
44. May JP, Hysi E, Wirtzfeld LA, Undzys E, Li SD, Kolios MC. Photoacoustic imaging of cancer treatment response: Early detection of therapeutic effect from thermosensitive liposomes. *PLoS One*. 2016; 11(10): e0165345.
45. Baumann R, Depping R, Delaperriere M, Dunst J. Targeting hypoxia to overcome radiation resistance in head & neck cancers: Real challenge or clinical fairytale? *Expert Rev Anticancer Ther*. 2016; 16(7): 751-8.